H_∞ tuning rules for positive position feedback controllers: the single-degree-of-freedom case and beyond

Jennifer Dietrich[1], Ghislain Raze[1], Arnaud Deraemaeker[2], Christophe Collette[3,4] and Gaëtan Kerschen[1]

Abstract

This paper presents an exact H_∞ tuning methodology for a positive position feedback (PPF) controller applied to a single-degree-of-freedom (SDOF) system. To this end, an equivalence between the closed-loop receptances of a PPF controller and a resistive-inductive shunt with a negative capacitance is put forward, which, in turn, enables us to adopt the existing shunt tuning rule in the active control case. The resulting tuning procedure is demonstrated using two numerical examples, namely an SDOF system and a finite element model of a cantilever beam. Based on the results obtained on the cantilever beam, it is shown that the influence of higher-frequency modes cannot be neglected to obtain effective vibration damping. The design procedure proposed for the PPF controller is then extended to this case and validated using an experimental cantilever beam.

Introduction

The attenuation of structural vibration is a well-known engineering problem. Today, mechanical structures tend to be more and more lightweight, which results in low structural damping and increased susceptibility to fatigue. One way to tackle this problem is to control the structure using an active damping device. Classical active control approaches are the direct velocity feedback (Balas 1979) and the integral force feedback (Preumont et al. 1992). An interesting alternative is a digital shunt absorber whose control authority can be enhanced with a negative capacitance (NC) (Fleming and Moheimani 2005; de Marneffe and Preumont 2008).

Another popular approach for active control is positive position feedback (PPF) (Goh and Caughey 1985; Fanson 1987; Fanson and Caughey 1990). In this approach, the structure's dynamics are attenuated by a compensator that controls the displacement with an actuation force and acts like a filter. This controller takes its name from the fact that the position coordinate measured by a sensor is both positively fed to the compensator and fed back to the structure via an actuator (Fanson and Caughey 1990; Agnes 1997). For a second-order PPF strategy, the controller function comprises three parameters, namely the pole frequency, the damping ratio and the controller gain. An advantage of PPF is that it can be designed based on an experimental transfer function so that no analytical model of the structure is needed. In addition, given its low-pass filter characteristic, the controller rolls off at higher frequency, and, hence, does not risk to excite residual modes (Inman 2006). Through a comparison between velocity feedback and PPF, Goh and Caughey (1985) pointed out that the

system stability can be more easily guaranteed with the latter approach. A downside of PPF controllers is that they induce low-frequency softening.

To design the PPF controller, a maximum attainable closed-loop damping strategy in combination with tuning filters in the multimodal case can be adopted (Goh and Caughey 1985). Dosch et al. (1992b) designed a self-sensing PPF controller using piezoelectric transducers acting as sensor and actuator at the same time. To choose adequate controller parameters, they used an optimization algorithm seeking optimal damping of the plant resonance (Dosch et al. 1992a,b). Kwak and Han (1998) used genetic algorithms to choose the PPF parameters (Kwak and Han 1998). However, only the controller frequency was varied therein while the other parameters were kept constant. PPF controllers are also

[1]Space Structures and Systems Laboratory (S3L), University of Liège, Quartier Polytech 1 (B52/3), Allée de la Découverte 9, 4000 Liège, Belgium

[2]Building Architecture and Town Planning (BATir) Department, Université Libre de Bruxelles, CP 194/02, av Franklin Roosevelt 50, 1050 Brussels, Belgium

[3]Active Aerospace Structures and Advanced Mechanical Systems, Université de Liège, Quartier Polytech 1 (B52/3), Allée de la Découverte 9, 4000 Liège, Belgium

[4]BEAMS Department, Université Libre de Bruxelles, Campus du Solbosch - CP 165/14, Avenue F.D. Roosevelt 50, 1050 Bruxelles, Belgium

Corresponding author:

Jennifer Dietrich, Department of Aerospace and Mechanical Engineering, University of Liège, Allée de la Découverte 9, 4000 Liège, Belgium

Email: jdietrich@uliege.be

often tuned to resonate at the natural frequency of the host structure so that the main focus is on the pole frequency (Huertas and Rohaľ-Ilkiv 2012). If a maximum flatband response is targeted, the PPF controller can be designed by means of a fifth-order Butterworth filter for a specific frequency as it was done by Russell et al. (2016).

Recent works aimed to provide systematic and effective tuning rules for PPF controllers, all the while limiting the undesirable low-frequency softening effects. Paknejad et al. (2020) optimized all three controller parameters based on maximum damping. In order to limit the softening introduced at low frequencies, they minimized the H_2 norm of the response during the final design. Their findings were demonstrated both numerically and experimentally. Another way to tackle the increased static response is to express the PPF filter in a fractional-order format (Marinangeli et al. 2018; Niu et al. 2018). If the system dynamics are well known, one could also add a feedforward control to counteract the increasing static response (Mokrani 2022). A thorough study of the interplay between desired damping performance, the static softening and system stability was presented by MacLean et al. (2022). Visalakshi et al. (2021) recently showed that PPF controllers can be tuned with a pole placement method with guaranteed stability properties. PPF controllers were also used in an adaptive setting (Saeed et al. 2021), with advanced composite (Silva et al. 2023) and aerospace (Gülbahçe and Çelik 2023; Yuan et al. 2024) structures, and with nonlinear systems (Zhao et al. 2019; Hamed et al. 2020; Saeed et al. 2021; Amer et al. 2022). Of special interest for this work is that of Zhao et al. (2019), which proposed to tune the PPF controller by adapting the fixed-point theory developed by Den Hartog for tuned mass dampers. The receptance of the controlled system thus features two peaks of approximately equal amplitude in place of the targeted resonance. However, this approach does not provide an exact solution in the H_∞ sense.

A PPF controller usually targets a specific resonance frequency of the host system. However, a real system cannot always be accurately described as a single-degree-of-freedom (SDOF) system; it is thus desirable to account for the influence of other structural modes during the tuning process. From a modeling perspective, for collocated control, Clark (1997) proposed to account for their influence by directly adding a feedthrough term to a state-space model that includes the overall displacement contribution of the out-of-bandwidth modes. Optionally, they suggested adding a second-order system in parallel to the model of the truncated system, simulating a single out-of-bandwidth mode representative of the other-mode dynamics. These corrections were shown to replicate the pole-zero pattern of the full system more faithfully. The influence of higher-order modes is also of crucial importance from the tuning perspective. Hoffmeyer and Høgsberg (2020) added a fictitious stiffness to simplify the system. The stiffness was then used to tune a PPF controller and to successfully introduce system damping in a numerical model. Fenik, S. and Starek, L. (2008) accounted for the influence of higher-order modes by including a constant as a correction of the controller gain in their formulas for the optimal controller parameters. They achieved maximum closed-loop damping

but expressed the controller gain as a function of the controller frequency and damping ratio. Additionally, they presented a multimodal PPF strategy where they accounted for the influence of each PPF controller in descending order with respect to their natural frequencies (Fenik, S. and Starek, L. 2008). There also exist approaches to account for the influence of higher-order modes in piezoelectric shunt damping by exploiting the dynamic capacitance function (Berardengo et al. 2016; Høgsberg and Krenk 2017; Raze et al. 2021).

In spite of a number of successful advanced applications, there still remains fundamental aspects on the PPF tuning currently unaddressed in the literature. First, to the authors' knowledge, there exists no closed-form solution to the H_∞ optimization problem in the case of a SDOF structure with a PPF controller. Second, a method such as that of Fenik, S. and Starek, L. (2008) allowing to extend simple SDOF tuning rules to the MDOF context is extremely useful for quick and effective tuning. Yet, the latter is limited to the pole placement problem. This work aims to solve these issues by drawing results from the research field of piezoelectric shunts. Interestingly, Agnes (1997) was the first to point out a dynamical similarity between a resistive-inductive (RL) shunt and a PPF controller. In fact, there exists a full equivalence between the receptance functions of an RL shunt with an NC and of a PPF controller, as will be shown in this work. Building upon this equivalence, a new optimal controller design aiming at equal peaks of the controlled receptance function is proposed for the PPF. This work can be seen as a continuation of a conference paper (Dietrich et al. 2022), making it applicable to multiple-degree-of-freedom (MDOF) structures and providing an experimental validation. Specifically, the original contributions of this work are as follows:

a) The equivalence of the closed-loop receptances of SDOF structures controlled by an RL shunt with an NC or by a PPF controller is mathematically demonstrated, suggesting that identical performance can be attained by the two approaches.

b) The coefficients of the receptances are functions of the tunable parameters. Using the aforementioned equivalence, exact H_∞ tuning rules are extended to the PPF to find the optimal values of the tunable parameters. In particular, it is shown that there exists a gain value that leads to a global minimum of the H_∞ norm.

c) For practical applications, these tuning rules are adapted to account for the influence of non-resonant modes in the MDOF case in an approximate way. This simple yet effective correction can substantially improve performance and without need for complex numerical optimization procedures. We will also show that the correction factors can be easily extracted from plant transfer functions.

d) These adapted tuning rules are eventually numerically and experimentally demonstrated with a piezoelectric beam. It is also shown how they improve upon the state-of-the-art method for H_∞ optimization of Zhao et al. (2019) .

The proposed tuning rules and corrections for non-resonant modes are simple and usable with experimentally identified models, making them widely applicable.

This work is organized as follows. First, the exact H_∞ tuning rule is applied to an SDOF example to demonstrate its performance and to investigate the open-loop transfer function and stability margins. Second, through correction factors applied to all controller parameters, the procedure is extended to account for the influence of higher-frequency modes. The developments are validated both numerically and experimentally. Finally, the effectiveness and limitations of the proposed tuning rule in an MDOF context are discussed.

PPF controller tuning

An SDOF system with a PPF controller

For an SDOF structure, the equation of motion using the Laplace variable s is given by

$$mxs^2 + kx = f \, , \tag{1}$$

where x is the displacement, f is an external force, and m and k are the mass and stiffness of the mechanical system, respectively. We regard the case of a system controlled by a PPF controller, considering a collocated displacement sensor and voltage actuator. The equations of motion then read

$$\begin{cases} mxs^2 + kx = f + \omega_c^2 g_c u_c \\ (s^2 + 2\omega_c \zeta_c s + \omega_c^2)u_c = x \end{cases} . \tag{2}$$

The variables u_c, ζ_c, ω_c and g_c refer to the control signal, damping ratio, frequency and gain of the controller, respectively. Inserting the second line of equation (2) into the first line yields

$$(ms^2 + k)x = f + \frac{\omega_c^2 g_c x}{s^2 + 2\omega_c \zeta_c + \omega_c^2}. \tag{3}$$

Dividing equation (3) by x and forming its reciprocal results in the closed-loop receptance function

$$\frac{x}{f} = \left[ms^2 + k - \frac{\omega_c^2 g_c}{s^2 + 2\omega_c \zeta_c s + \omega_c^2} \right]^{-1} . \tag{4}$$

Using the definitions given by Ikegame et al. (2019),

$$x_{st} := \frac{f}{k}, \ \omega_0 := \sqrt{\frac{k}{m}}, \ \hat{s} := \frac{s}{\omega_0}, \ \nu_c := \frac{\omega_c}{\omega_0}, \ g := \frac{g_c}{k}, \tag{5}$$

equation (4) can be written in dimensionless form:

$$h(\hat{s}) = \frac{x}{x_{st}} = \left[\hat{s}^2 + 1 - \frac{g}{\frac{\hat{s}^2}{\nu_c^2} + 2\zeta_c \frac{\hat{s}}{\nu_c} + 1} \right]^{-1} . \tag{6}$$

An SDOF system with an RL shunt in series with an NC

The equations of motion of the piezoelectric SDOF structure connected to an RL shunt with an NC are given by

$$\begin{cases} mxs^2 + k_{oc}x - \theta q = f \\ \theta x - \frac{1}{C_p^\varepsilon} q = V \end{cases} . \tag{7}$$

q is the electrical charge of the electrodes of the piezoelectric transducer, and V is the voltage across them. k_{oc} is the system stiffness when the transducer is in open-circuit, and C_p^ε is the capacitance of the piezoelectric transducer under constant strain. The equations are coupled through the electromechanical coupling coefficient θ. This coefficient characterizes how much energy is transformed between the piezoelectric transducer and the mechanical system (Hagood and von Flotow 1991). In open-circuit ($q = 0$), the resonance frequency is $\omega_{oc} = \sqrt{k_{oc}/m}$. In short-circuit ($V = 0$), $\omega_{sc} = \sqrt{k_{sc}/m}$ where

$$k_{sc} = k_{oc} - \theta^2 C_p^\varepsilon. \tag{8}$$

A way to assess the electromechanical coupling is the dimensionless electromechanical coupling factor (EMCF) K_c, that relates the modal strain energies when the transducer is in short- and in open-circuit (Toftekær et al. 2020):

$$K_c^2 = \frac{\omega_{oc}^2 - \omega_{sc}^2}{\omega_{sc}^2} . \tag{9}$$

Thus, the coupling factor depends on the fixed properties of the host system through θ and C_p^ε. One could also normalize the coupling factor with ω_{oc}, defining the EMCF as

$$\alpha^2 = \frac{\omega_{oc}^2 - \omega_{sc}^2}{\omega_{oc}^2} = \frac{K_c^2}{1 + K_c^2} . \tag{10}$$

When the piezoelectric transducer is connected to an RL shunt circuit in series with a negative capacitance C_n, we obtain

$$\left(Ls^2 + Rs - \frac{1}{C_n} \right) q = V. \tag{11}$$

Thus, the electrical part of equation (7) reads

$$Ls^2 q + Rsq + \frac{1}{C_{eff}} q - \theta x = 0, \tag{12}$$

where the effective capacitance is (Berardengo et al. 2016)

$$\frac{1}{C_{eff}} = \frac{1}{C_p^\varepsilon} - \frac{1}{C_n}. \tag{13}$$

The transfer function from the force to the displacement is obtained from equations (7) and (12)

$$\frac{x}{f} = \left[ms^2 + k_{oc} - \frac{\theta^2}{Ls^2 + Rs + \frac{1}{C_{eff}}} \right]^{-1} . \tag{14}$$

Considering the electrical frequency and damping ratio of the shunt

$$\omega_e^2 := \frac{1}{C_{eff}L}, \ 2\omega_e \zeta_e := \frac{R}{L} \tag{15}$$

and (Ikegame et al. 2019)

$$x_{st} := \frac{f}{k_{oc}}, \ \tilde{\alpha}^2 := \frac{\theta^2 C_{eff}}{k_{oc}}, \ \nu_e := \frac{\omega_e}{\omega_{oc}}, \ \hat{s} := \frac{s}{\omega_{oc}} , \tag{16}$$

the transfer function of the SDOF system with the piezoelectric shunt can be expressed in dimensionless form

$$h(\hat{s}) = \frac{x}{x_{st}} = \left[\hat{s}^2 + 1 - \frac{\tilde{\alpha}^2}{\frac{\hat{s}^2}{\nu_e^2} + 2\zeta_e \frac{\hat{s}}{\nu_e} + 1} \right]^{-1} , \tag{17}$$

where tilde refers to the case when an NC is used.

From the dimensionless receptance functions in equations (6) and (17), we conclude that a PPF controller and an RL shunt with an NC are completely equivalent in terms of closed-loop receptance. The correspondence between the different parameters reads as follows

$$g \equiv \tilde{\alpha}^2, \quad \nu_c \equiv \nu_e, \quad \zeta_c \equiv \zeta_e . \tag{18}$$

Specifically, the gain of the PPF controller g corresponds to $\tilde{\alpha}$ which is related to the enhanced electromechanical coupling of the structure and is influenced directly by the NC.

The implications of this equivalence are discussed in depth in Dietrich et al. (2022) for an SDOF system. As was shown therein, the PPF results in much better stability margins than the RL shunt with an NC, which is why the former is the main focus of this work.

H_∞ optimization

Exact tuning rules for the H_∞ optimization of passive RL shunts were introduced by Soltani et al. (2014). Specifically, these rules are based on the optimization of the receptance of the controlled system. The optimal tuning results in two resonance peaks featuring identical amplitudes in the receptance function. As is well-known from the literature, adding an NC to this system leads to the same model class as in the case without NC (Berardengo et al. 2016). It was also shown herein that this same model class represents the case of a SDOF structure with a PPF controller. Therefore, both the NC and PPF optimization problems can be treated with the method of Soltani et al. (2014) (a similar philosophy was followed for electromagnetic shunts by Ikegame et al. (2019)). These results can directly be exploited to tune the parameters of a PPF controller, thereby providing an exact closed-form solution to the H_∞ control problem for the PPF case. The parameters for which there is an equivalence, namely g, ν_c and ζ_c can thus be optimized for the PPF. As for the NC, one can first optimize the parameters $\tilde{\alpha}^2$, ν_e and ζ_e, and deduce the shunt parameters C_n, R and L using equations (13) and (17).

Thanks to the incorporation of the controller gain g, there is however an additional free parameter in comparison with the passive RL shunt approach. First, we fix g to find optimal values for ν_c and ζ_c by minimizing the H_∞ norm of the transfer function $h(i\hat{\omega})$. Here, i is the imaginary number, and $\hat{\omega}$ is a circular frequency normalized by ω_0:

$$\min_{\nu_c, \zeta_c} \|h(i\hat{\omega}_c)\|_\infty$$
$$\rightarrow \text{find } \nu_c, \zeta_c \text{ such that } |h(i\hat{\omega}_{c,A})| = |h(i\hat{\omega}_{c,B})| \equiv h_0.$$

h_0 is the maximum amplification of the two equal resonance peaks located at dimensionless frequencies $\hat{\omega}_{c,A}$ and $\hat{\omega}_{c,B}$. h_0 is expressed as a function of g (Soltani et al. 2014):

$$h_0 = \frac{8}{\sqrt{g}\sqrt{2\sqrt{54g^2 - 144g + 64} + 9g + 16}} \tag{19}$$

which yields

$$135h_0^4 g^4 - 864h_0^4 g^3 + 1152h_0^2 g^2 + 2048h_0^2 g - 4096 = 0. \tag{20}$$

This quartic equation in g can be solved in closed form so that the gain g can be determined from a desired amplification h_0. The peak amplitude h_0 is now minimized. Using Mathematica (Wolfram Research Inc. 2022):

$$\frac{\partial h_0}{\partial g} = -\frac{4\left(\frac{216g^{3/2} - 288\sqrt{g}}{\sqrt{54g^2 - 144g + 64}} + 18\sqrt{g}\right)}{\sqrt{g}\left(9g + 2\sqrt{54g^2 - 144g + 64} + 16\right)^{3/2}}$$
$$-\frac{8}{g\sqrt{9g + 2\sqrt{54g^2 - 144g + 64} + 16}}. \tag{21}$$

Equating this derivative to zero eventually yields the value g_{opt} that minimizes the peak amplitude h_0,

$$g_{opt} = \frac{8}{15} = 0.5333 . \tag{22}$$

The minimum attainable H_∞ norm can be found by inserting g_{opt} in equation (19):

$$h_{0,opt} = \sqrt{5}. \tag{23}$$

Using g_{opt}, the parameters ν_c and ζ_c can now be found. For the shunt, they are expressed as a function of the coupling factor in Soltani et al. (2014). For the PPF controller, we introduce $K^2 = \frac{g}{1-g}$ and apply the tuning rules provided by Soltani et al. (2014). With the intermediate parameter

$$r = \frac{\sqrt{64 - 16K^2 - 26K^4} - K^2}{8}, \tag{24}$$

the optimal frequency and damping ratios are

$$\nu_c = \sqrt{\frac{3K^2 - 4r + 8}{4K^2 + 4}} \tag{25}$$

and

$$\zeta_c = \frac{\sqrt{27K^4 + 80K^2 + 64 - 16r\left(4 + 3K^2\right)}}{\sqrt{2}\left(5K^2 + 8\right)}, \tag{26}$$

respectively.

Performance and stability investigations

The performance of the derived PPF tuning rule is demonstrated herein. Both the open-loop transfer function and the stability of the controlled system are investigated.

Performance

The transfer functions between the structural response and the external force are compared in Figure 1 in the uncontrolled (equation (1)) and controlled (equation (6)) cases. The optimal case is represented by (━━). Thanks to the PPF, the original resonance peak has been replaced with two resonance peaks featuring much lower — and equal — amplitudes. However, we also observe that the controller increases the static response which is confirmed by the formula (cf. equation (6))

$$h(0) = \frac{1}{1-g}. \tag{27}$$

(a) FRFs for $g = 0.85g_{opt}$ (━━), $g = g_{opt}$ (━━) and $g = 1.046g_{opt} = g_{max}$ (━━).

(b) FRFs for $g = 0.2g_{opt}$ (━━), $g = 0.5g_{opt}$ (━━), $g = 0.75g_{opt}$ (━━) and $g = g_{opt}$ (━━).
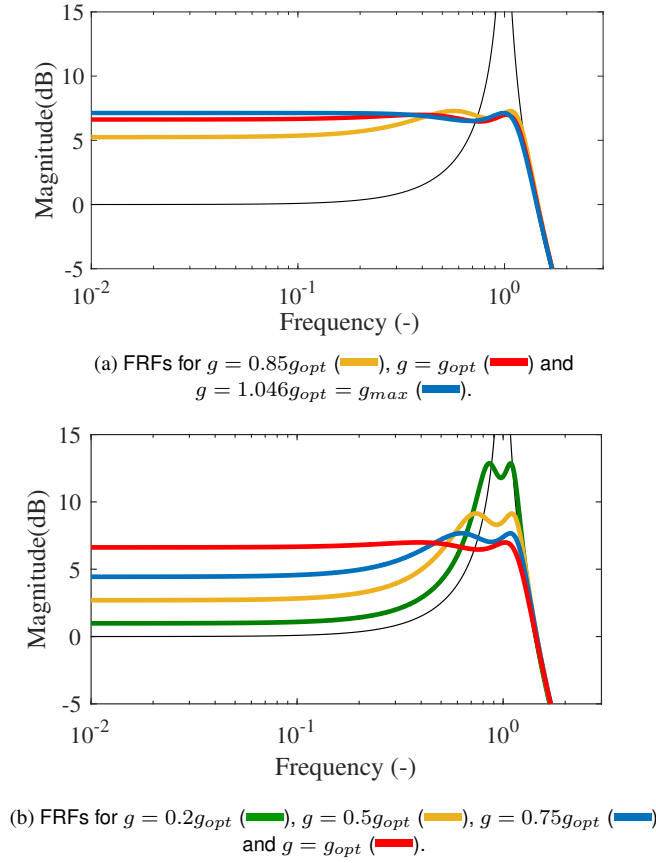
Figure 1. FRFs between the structural response and the external disturbance voltage of the SDOF system controlled by a PPF controller with different gain settings. The uncontrolled response is represented with (━━).

Frequency response functions (FRFs) for different values of the gain are displayed in Figure 1. If $g < g_{opt}$, the static response is smaller than in the optimal case but the magnitude of the resonance amplitude is greater.

Soltani et al. (2014) stated that the α for shunts should not be chosen higher than $\tilde{\alpha}_{max} = 0.74815$ to guarantee an equal-peak design. This translates into $g_{max} = 0.5597$ for the PPF controller. Figure 2 compares the maximum amplitude of the receptance function h_0 with the amplitude of the static response for different values of the gain g. Indeed, when $g > g_{max}$, the maximum of the receptance function is shifted to $\hat{s} = 0$. The minimum amplitude in equation (23) obtained for g_{opt} is thus an absolute minimum. In addition, the H_2 norm of the FRF response is presented in Figure 2. It can be observed that it decreases in a relatively similar fashion to the H_∞ norm; however, the minimum of the H_2 norm occurs for a lower value of the gain (g ≈ 0.49).

For the fixed-points-based method from Zhao et al. (2018, 2019), the gain needs to be chosen according to a trade-off between the static softening and the amplitude reduction. Zhao et al. stated that, for ideal performance, the gain should be chosen as large as possible while respecting the stability limit. However, doing so will substantially enlarge the static
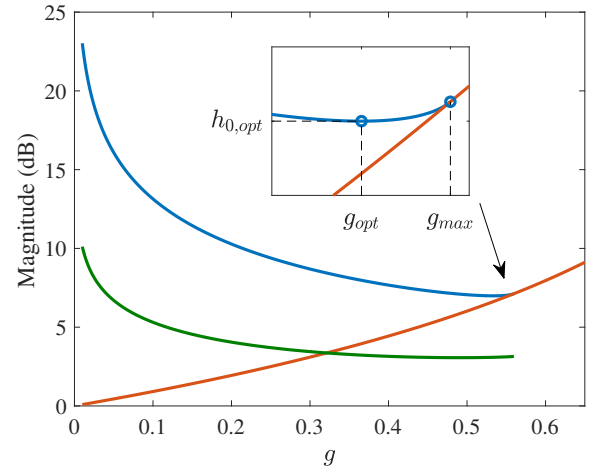

Figure 2. Maximum amplitude h_0 (━━), H_2 norm of the FRF amplitude (━━), and static response (━━) of the controlled SDOF system as a function of the gain g.

response of the controller so that, eventually, g needs to be smaller. It is set to g_{opt} herein. The comparison with the proposed tuning rule is displayed in Figure 3. It can be seen that the fixed-points method does not yield resonance peaks with equal amplitude whereas the static responses are identical, and the resulting H_∞ norm is lower.
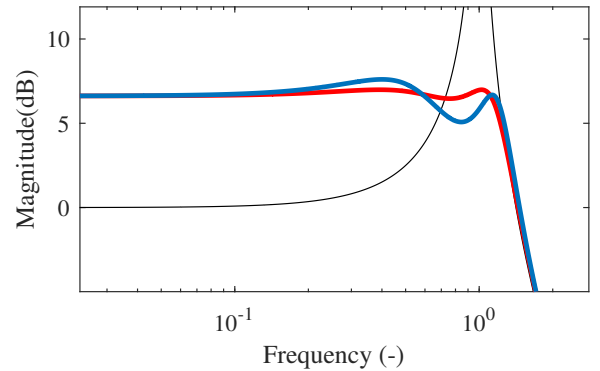

Figure 3. FRFs between the structural response and external force of an SDOF system. Uncontrolled (━━), controlled by a PPF controller with exact H_∞ rules (━━) and by a tuning based on fixed points (━━).

Stability and stability margins

In order to explain the stability of the controlled system, we consider the open-loop transfer function for a plant G_{PPF} controlled by a PPF controller, expressed as

$$H_{ol,PPF}(\hat{s}) = -G_{PPF}(\hat{s})PPF(\hat{s}). \qquad (28)$$

The plant transfer function $G_{PPF}(s)$ is the transfer function between the controller force $f_{PPF} = \omega_c^2 g_c u_c$ and the displacement x when $f = 0$:

$$G_{PPF}(s) = \frac{1}{ms^2 + k}. \qquad (29)$$

The PPF controller function is the second-order filter

$$PPF(s) = \frac{g_c \omega_c^2}{s^2 + 2\omega_c \zeta_c s + \omega_c^2}. \qquad (30)$$
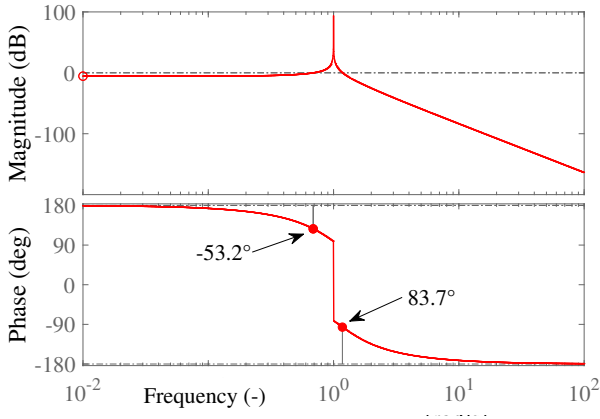
Figure 4. Bode plot of the open-loop transfer function of a dimensionless SDOF system with a PPF controller tuned according to the H_∞ tuning rule. Decisive phase margins are indicated with a •.

Using equations (29) and (30), and the parameters in equation (5), the open-loop transfer function in dimensionless form is

$$\begin{aligned} H_{ol,PPF}(\hat{s}) &= -G_{PPF}(\hat{s})PPF(\hat{s}) \\ &= -\frac{1}{\hat{s}^2 + 1}\frac{g}{\frac{\hat{s}^2}{\nu_c^2} + 2\zeta_c\frac{\hat{s}}{\nu_c} + 1}. \end{aligned} \quad (31)$$

Previous works have shown that as long as the damping ratio and optimal frequency are greater than zero, the only parameter that could destabilize the controller is g (de Marneffe and Preumont 2008; Zhao et al. 2018). A stability limit is reached when the structure's stiffness is counterbalanced by the controller gain. Krenk and Høgsberg (2013) derived the stability criterion directly using the stiffness matrix, stating that the stiffness of the structure (in the MDOF case, including higher-order modes) must be greater than the gain factor(s). For the SDOF case, this criterion then condenses into a scalar. Zhao et al. (2018) defined the stability limit for the gain of a PPF controller by $g < 1$. In the context of the shunt analogy, the addition of an NC into the circuit can be interpreted as introducing a negative stiffness to the system. Similarly to the PPF controller, the system then becomes unstable if the negative stiffness of the transducer cancels out the structure's stiffness (as it is seen from the transducer) (de Marneffe and Preumont 2008). A detailed discussion of the analogy with respected to the system stability can be found in Dietrich (2023).

Closed-loop stability is a necessary requirement to guarantee the performance of a control system but it is not a sufficient one. In practice, one has to ensure sufficient stability margins to account for uncertainties and unmodeled dynamics in the system. These margins can be deduced from the open-loop transfer functions (Franklin et al. 1990). The Bode plot of the open-loop transfer function in the tuned case in Figure 4 features a phase margin of $-53.2°$ or $83.7°$, which can be considered as acceptable. It should be noted that a negative phase margin in this case does not result in an unstable system. It rather means that if the system undergoes a phase lead (and not lag) modification it will become unstable, as can be deduced from Figure 4. We note that the open-loop transfer function in the optimal case

features the smallest phase margin and that all variations of the controller gain g leave sufficient phase margins for a viable use in practical applications.

Extension to MDOF systems

In the previous sections, the tuning rule was established for an SDOF host structure. This section considers the MDOF case. In this context, the main idea is to tune the parameters of the PPF controller in order to minimize the H_∞ norm of the modal amplitude of the targeted mode. The influence of other modes is taken into account via correction factors of the controller parameters. The proposed correction method is based on developments for piezoelectric vibration absorbers (Berardengo et al. 2016; Raze et al. 2022) and adapted to the active control case. It also shares similarities with the method of Fenik, S. and Starek, L. (2008), but is not limited to a pole placement problem.

Accounting for higher-order modes

The equations of motion in modal space of an MDOF system with a PPF controller are:

$$\begin{cases} (s^2\mathbf{I} + \mathbf{\Omega}^2)\boldsymbol{\eta} = \mathbf{f} + \mathbf{w}\omega_c^2 g_c u_c \\ (s^2 + 2\zeta_c\omega_c s + \omega_c^2)u_c = \omega_c^2 g_c x_s \ , \\ x_s = \mathbf{v}^T\boldsymbol{\eta} \end{cases} \quad (32)$$

where $\mathbf{v}^T$ and $\mathbf{w}$ are vectors indicating the position of the sensor and of the actuator, respectively. $\mathbf{I}$ is the identity matrix, and $\mathbf{\Omega}$ is a diagonal matrix with the resonance frequencies. $\boldsymbol{\eta}$ is the vector of modal amplitudes, and x_s is the sensor signal. $\boldsymbol{\eta}$ is partitioned such that

$$\boldsymbol{\eta}^T = [\, \boldsymbol{\eta}_{<i}^T,\, \eta_i,\, \boldsymbol{\eta}_{>i}^T\,]. \quad (33)$$

Here, the subscript i stands for the targeted mode so that $\boldsymbol{\eta}_{<i}$ and $\boldsymbol{\eta}_{>i}$ include the modal amplitudes of lower and higher frequency modes, respectively. Vectors $\mathbf{v}$ and $\mathbf{w}$ are likewise partitioned as

$$\mathbf{v}^T = [\, \mathbf{v}_{<i}^T,\, v_i,\, \mathbf{v}_{>i}^T\,] \quad \text{and} \quad \mathbf{w}^T = [\, \mathbf{w}_{<i}^T,\, w_i,\, \mathbf{w}_{>i}^T\,]. \quad (34)$$

For the following considerations, we set $\mathbf{f} = 0$. For $\boldsymbol{\eta}_{<i}$, one can assume that the dominant term of the first line of equation (32) is

$$s^2\boldsymbol{\eta}_{<i} = \mathbf{w}_{<i}\omega_c^2 g_c u_c \quad (35)$$

as, in this frequency range, $\mathbf{\Omega}$ is small in relation to $s^2\mathbf{I}$. As for $\boldsymbol{\eta}_{>i}$, one obtains

$$\mathbf{\Omega}^2\boldsymbol{\eta}_{>i} = \mathbf{w}_{>i}\omega_c^2 g_c u_c, \quad (36)$$

neglecting the $s^2\mathbf{I}$ term. The sensed signal x_s can be expressed with equation (33), so that

$$x_s = \mathbf{v}_{<i}^T\boldsymbol{\eta}_{<i} + v_i\eta_i + \mathbf{v}_{>i}^T\boldsymbol{\eta}_{>i}. \quad (37)$$

Inserting equations (35) and (36) in equation (37) yields

$$x_s = \frac{1}{s^2}\mathbf{v}_{<i}^T\mathbf{w}_{<i}\omega_c^2 g_c u_c + v_i\eta_i + \mathbf{v}_{>i}^T\mathbf{\Omega}^{-2}\mathbf{w}_{>i}\omega_c^2 g_c u_c. \quad (38)$$

Introducing the auxiliary variables

$$\frac{\kappa_{<i}}{s^2} = \mathbf{v}_{<i}^T\frac{1}{s^2}\mathbf{w}_{<i} \quad \text{and} \quad \kappa_{>i} = \mathbf{v}_{>i}^T\mathbf{\Omega}^{-2}\mathbf{w}_{>i}, \quad (39)$$

the insertion of equation (38) into equation (32) gives

$$\begin{cases} (s^2 + \omega_i^2)\eta_i = w_i\omega_c^2 g_c u_c \\ \left(s^2 + 2\zeta_c\omega_c s + \omega_c^2 - \omega_c^2 g_c \kappa_{>i} - \omega_c^2 g_c \kappa_{<i}\dfrac{1}{s^2} \right) u_c = v_i\eta_i \end{cases}$$
(40)

In the experiments conducted in this work, the first structural mode is targeted. Thus, $\kappa_{<i} = 0$. If higher-order modes were targeted, one could as a first approximation also neglect its associated term, given that its magnitude decays with the square of the frequency. Introducing now the parameters

$$\hat{u}_c = \frac{u_c}{v_i}, \quad \hat{\omega}_c^2 = \omega_c^2 - \omega_c^2 g_c \kappa_{>i},$$
$$\hat{g}_c = \frac{\omega_c^2 g_c w_i v_i}{\hat{\omega}_c^2}, \quad \hat{\zeta}_c = \frac{\zeta_c \omega_c}{\hat{\omega}_c},$$
(41)

equation (40) becomes

$$\begin{cases} (s^2 + \omega_i^2)\eta_i = \hat{\omega}_c^2 \hat{g}_c \hat{u}_c \\ \left(s^2 + 2\hat{\zeta}_c\hat{\omega}_c s + \hat{\omega}_c^2 \right) \hat{u}_c = \eta_i \end{cases},$$
(42)

which has the same form as equation (2). The tuning formulas given in equations (22) and (24) - (26) can thus be used to tune the controller parameters. Using equation (41), we can then express the corrected PPF controller parameters as:

$$g_c = \frac{\hat{g}_c}{v_i w_i + \kappa_{>i}\hat{g}_c}, \quad \omega_c^2 = \frac{\hat{\omega}_c^2}{1 - g_c \kappa_{>i}}, \quad \zeta_c = \frac{\hat{\zeta}_c\hat{\omega}_c}{\omega_c}.$$
(43)

The tuning procedure for the PPF controller in the MDOF case is as follows:

1. Identification of the system parameters ω_i, w_i, v_i and $\kappa_{>i}$.
2. Computation of the optimal PPF controller parameters $\hat{\omega}_c, \hat{\zeta}_c$ and $\hat{g}_c$, using ω_i as in an SDOF case according to the previously defined tuning rules.
3. Correction of the controller parameters according to equation (43).

An advantage of this on-hand methodology is that it is widely and conveniently applicable since the identification of the system parameters can be easily achieved with state-of-the-art methods. In comparison to Clark (1997), it can be used for different sensor-actuator configurations. However, the equal-peak design is only enforced on one modal coordinate, and the corrections depend on the considered plant transfer function. Thus, an equal-peak design cannot be guaranteed a priori, and the performance depends on the considered input and output locations.

Numerical demonstration on a cantilever beam

The structure chosen to demonstrate the previous developments numerically and experimentally is the cantilever steel beam with a thin lamina at its free end schematized in Figure 5. The beam comprises ten piezoceramic patches on each side of the beam. This structure was the subject of other studies, often in a clamped-clamped configuration to trigger the nonlinearity of the thin lamina (see, e.g., Raze et al.
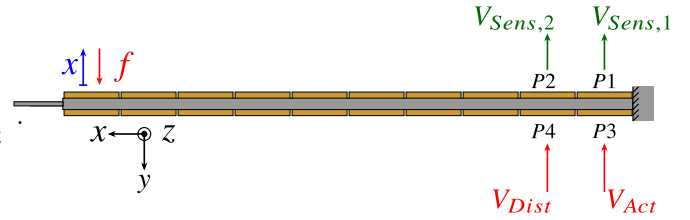

Figure 5. Top view on the cantilever beam setup.

(2020, 2022)). In this study, the clamping of the thin lamina is freed to remain in a linear regime of motion.

For the model, a steel beam ($700\,\text{mm} \times 14\,\text{mm} \times 14\,\text{mm}$) with a thin steel lamina ($100\,\text{mm} \times 14\,\text{mm} \times 0.5\,\text{mm}$) and with piezoceramic patches of the type PSI-5A4E is considered. Two piezoelectric patches, namely $P1$ and $P2$, act as voltage sensors, both on one side and close to the clamping. The patch $P3$ functions as a voltage actuator of the controller and $P4$ as a voltage actuator imposing a disturbance voltage to the structure. The displacement is measured at the end of the cantilever beam.

A finite element (FE) model with Euler-Bernoulli beam elements was built based on the method proposed by Thomas et al. (2009), considering three DOFs per node (axial, transversal, rotation), accounting for displacements along the x- and y-axis and rotations around the z-axis (cf. Figure 5). The other DOFs were neglected as their motions were considered negligible; more sophisticated and accurate 2D or 3D models could be built but this was not deemed necessary given the good agreement of the numerical model with experimental results. Both the beam and the lamina were discretized with one element per millimeter, yielding a model with 4437 DOFs. For simplification, a Craig-Bampton-based model order reduction was used according to the technique in Raze et al. (2022). One interface mechanical DOF and all electrical DOFs for the patches were retained together with 20 vibration modes. Modal damping of $0.2\,\%$ was added in the model. To assess control performance, the transfer functions from the disturbance voltage to the tip displacement are regarded. In addition, the transfer functions from a disturbance force at the beam tip to the tip displacement are also taken into account.

Plant transfer functions

In control theory, a collocated sensor-actuator pair is always preferable since it is accompanied by an alternating pole-zero pattern in the open-loop transfer function, which offers good stability margins (Preumont 2011). The plant transfer function of pseudo-collocated ($P1$ to $P3$) and non-collocated ($P2$ to $P3$) configurations are displayed in Figure 6. The $P1$ to $P3$ case corresponds to two piezoelectric patches placed at the same location, but on either side of the beam. It is referred to as pseudo-collocated, because transversal in-plane motions may cause a disturbance to the alternating pole-zero pattern at high frequencies. For simplicity, this case will be referred to as collocated in what follows. Nonetheless, both configurations feature an alternating pole-zero pattern, although this feature is certainly not generic for non-collocated cases.
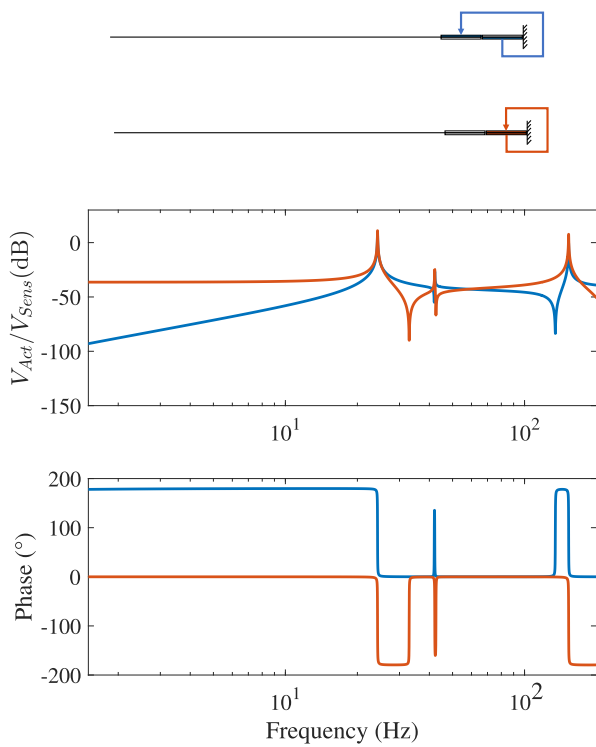
Figure 6. Bode plot of the plant transfer functions of the numerical beam. Non-collocated ($P2$ to $P3$) (━━) and pseudo-collocated ($P1$ to $P3$) (━━).

In this numerical experiment, our target is the first mode, which corresponds to the first bending mode of the cantilever beam. The identified resonance frequencies are $24.28\,\text{Hz}$, $42.13\,\text{Hz}$ and $152.9\,\text{Hz}$ for modes #1 - #3, respectively. Figure 6 shows that the first two poles are relatively close to each other. Therefore, an SDOF approximation of the first mode might not be adequate for the tuning process.

Collocated versus non-collocated setups The performance of the PPF controller designed according to the proposed H_∞ tuning rule is displayed in Figure 7. In Figure 7(a), a disturbance voltage is acting via $P4$. Both configurations yield a substantial resonance amplitude reduction (around $40\,\text{dB}$), but only the non-collocated configuration exhibits a strong amplification of the static response. Indeed, the piezoelectric actuator applies a torque which only impacts the beam section of $P4$ (the in-plane displacements are assumed to be small herein). So, in the static case, only the sensor at $P2$ can sense the disturbance and activate the controller. We also note that the two resonance peaks visible in Fig. 3 are much harder to see here because of the increased static response and the perturbation due to the higher-frequency modes.

A disturbance force at beam tip is now considered in Figure 7(b). The performance in similar in both configurations leading to an amplitude reduction of $47\,\text{dB}$. Because the disturbance force at beam tip mostly activates the first bending mode, the influence of the other modes is reduced, and two equal peaks can be enforced by the controller. These observations demonstrate the impact of the choice of the transfer function on performance assessment.
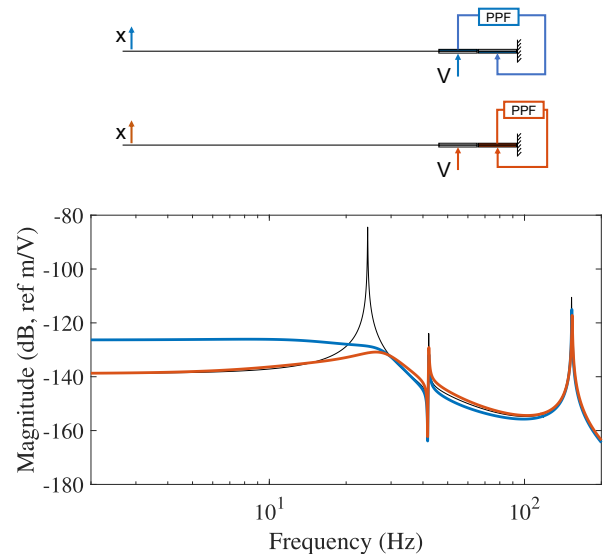
(a) From disturbance voltage ($P4$) to tip displacement.
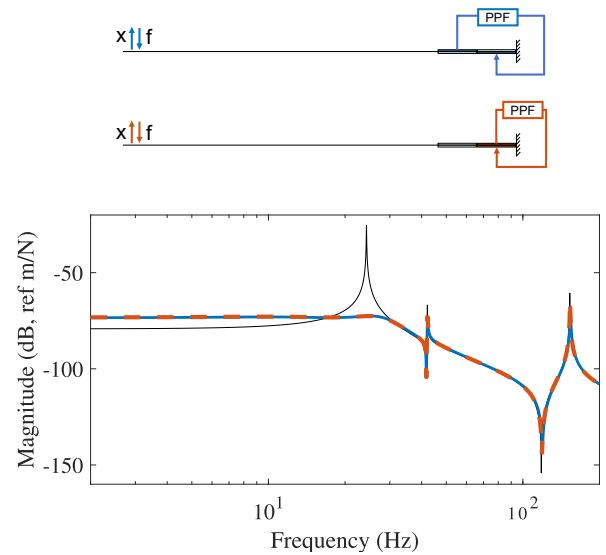
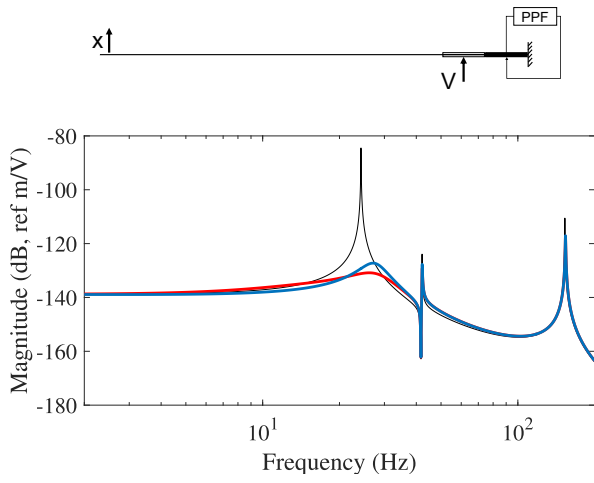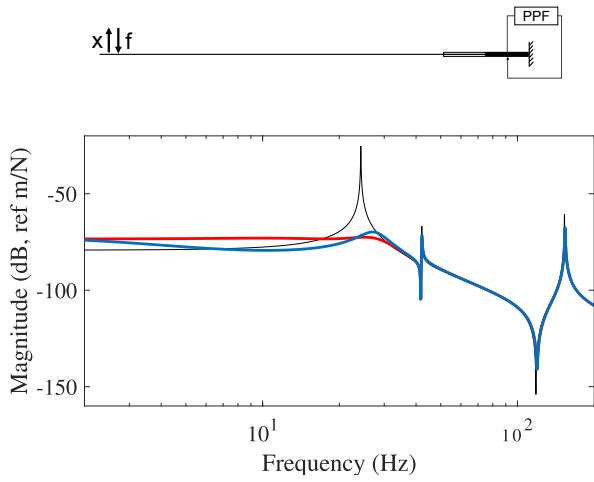(b) From disturbance force at the beam tip to tip displacement.

Figure 7. FRFs of the numerical beam. Uncontrolled (━━); controlled by a PPF accounting for the influence of higher-order modes in a non-collocated (━━) and pseudo-collocated (━━) setup.

The influence of higher modes

Figure 8 compares the receptance functions for the uncontrolled system, as well as the controlled system with a PPF controller tuned with and without higher-mode correction (collocated case). The correction leads to an improvement of $5.5\,\text{dB}$ and $3.5\,\text{dB}$ in Figures 8 (a,b), respectively. In addition, the PPF controller is strongly detuned when higher modes are neglected, because a resonance peak remains in the frequency range of interest.

Variations of the controller gain

The variation of the controller gain is now studied for the collocated controller, similar to what was achieved in Figure 1. Figure 9 presents what happens for a small variation of g. For a disturbance voltage, we observe an imbalance

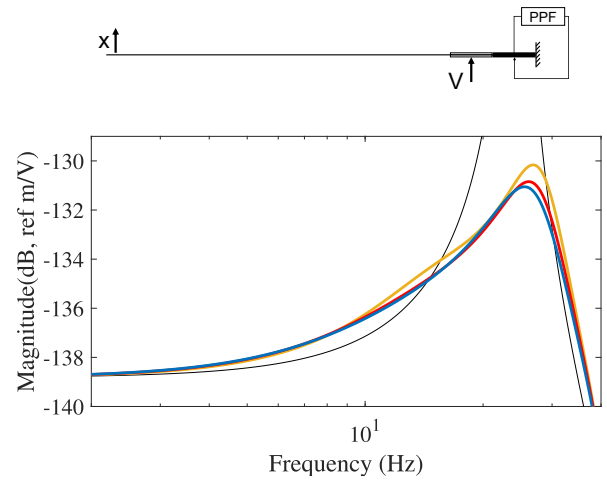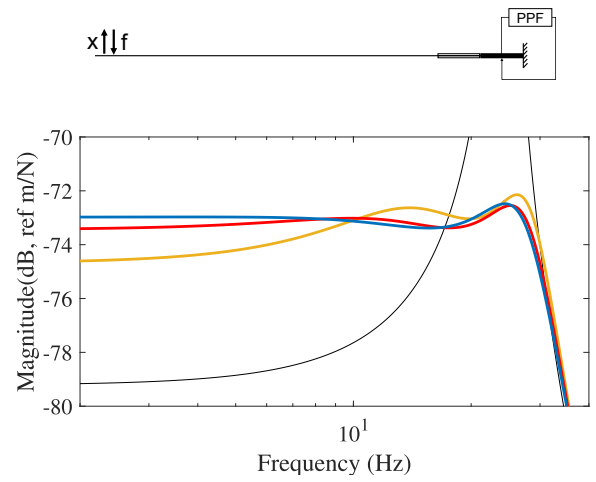(a) From disturbance voltage ($P4$) to tip displacement.

(b) From disturbance force at the beam tip to tip displacement.

Figure 8. FRFs of the numerical beam. Uncontrolled (━━);
PPF controller accounting for higher-order modes (━━)
or not (━━).

(a) From disturbance voltage ($P4$) to tip displacement.

(b) From disturbance force at the beam tip to tip displacement.

Figure 9. FRFs between the structural response and the
external disturbance voltage of the numerical beam controlled
by a PPF with different gains (uncontrolled response: ━━).
Gain variations of $g = 0.85g_{opt}$ (━━), $g = g_{opt}$ (━━) and
$g = 1.046g_{opt} = g_{max}$ (━━).

between the two resonance peaks, even when the controller
is optimally tuned. As previously discussed, this is probably
due to the influence of other structural modes and to the static
response. Also, the optimally-tuned controller does not yield
the best damping performance in this example, probably
due to the fact that the static response is not amplified.
Considering now the receptance function from a disturbance
force to the tip displacement, an equal-peak design is better
approached. First, the static response is increased as it is
typical for the controller. Second, as already mentioned
before, the influence of the higher order modes is smaller
at this input location. In this transfer function, the theoretical
developments from the beforehand discussed SDOF system
can be reproduced, i.e., the controller with the optimal gain
leads to the best damping performance.

Comparison with the fixed-points method

Figure 10 compares the proposed tuning methodology with
a fixed-points tuning, both with correction for the higher
modes. The former is found to be slightly more effective,
increasing the damping performance by $1\,dB$. In addition,
considering Figure 10(b), the two peaks of the system with
the H_∞-based controller are better balanced. Based on these

results, it can be stated that the g_{opt} found in equation
(22) and the consideration of the higher-order modes does
not only lead to an enhancement of the exact but also of
the fixed-points tuning rule in the MDOF case. While the
difference between the two methods in terms of performance
(about $1\,dB$) might not be substantial, the method proposed
in this work provides a mathematically exact solution (for
the SDOF case) with an optimal gain value, including an
expression of the receptance amplitude.

Experimental demonstration on a cantilever beam

Experimental setup

The structure of interest corresponds to the beam used during
the numerical simulations. Figure 11 shows the experimental
setup. One piezoelectric patch located next to the clamping
was used as an actuator while the patch next to it was
used to excite the structure with a disturbance voltage.
The patches on the opposite side were used as sensors.
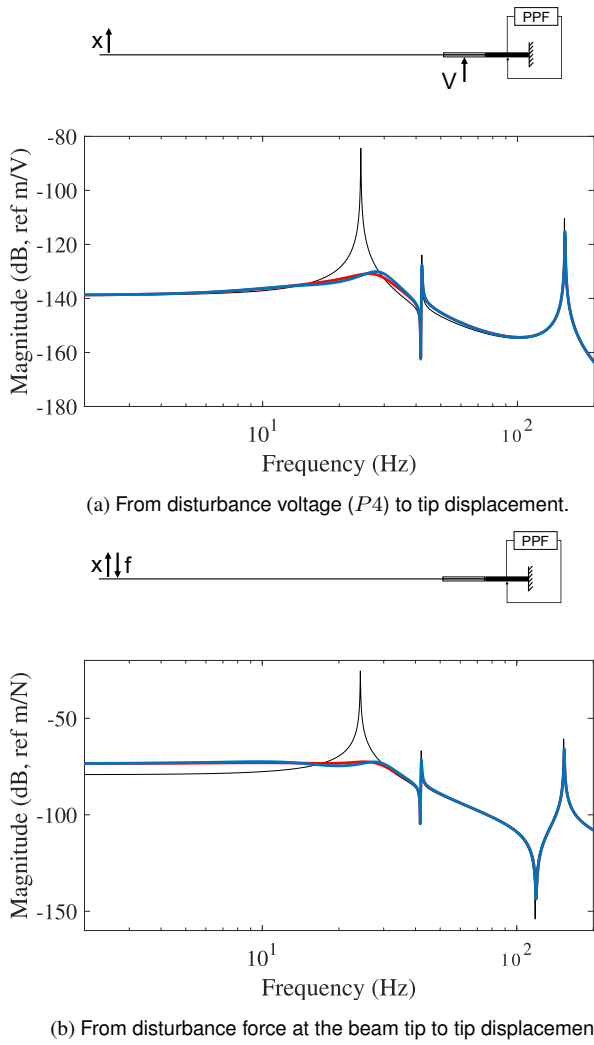Sensors 1 and 2 correspond to collocated and non-collocated

(a) From disturbance voltage ($P4$) to tip displacement.

(b) From disturbance force at the beam tip to tip displacement.

Figure 10. FRFs of the numerical beam. Uncontrolled (━━); controlled by a PPF controller tuning using H_∞ rule (━━) or the fixed-points method (━━).
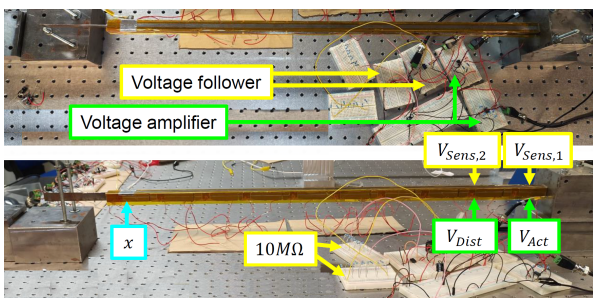

Figure 11. Experimental setup.

configurations, respectively. The amplitudes of the actuator and disturbances voltages were increased by a gain equal to 10 with a voltage amplifier. These gains are included in the graphical plots for comparison with the numerical results. The digital controller unit dSPACE MicroLabBox was used for the excitation signals, measurements and the implementation of the controller function. An accelerometer measured the response at beam tip. For comparison with the numerical simulations, this acceleration was integrated twice to obtain the displacement.
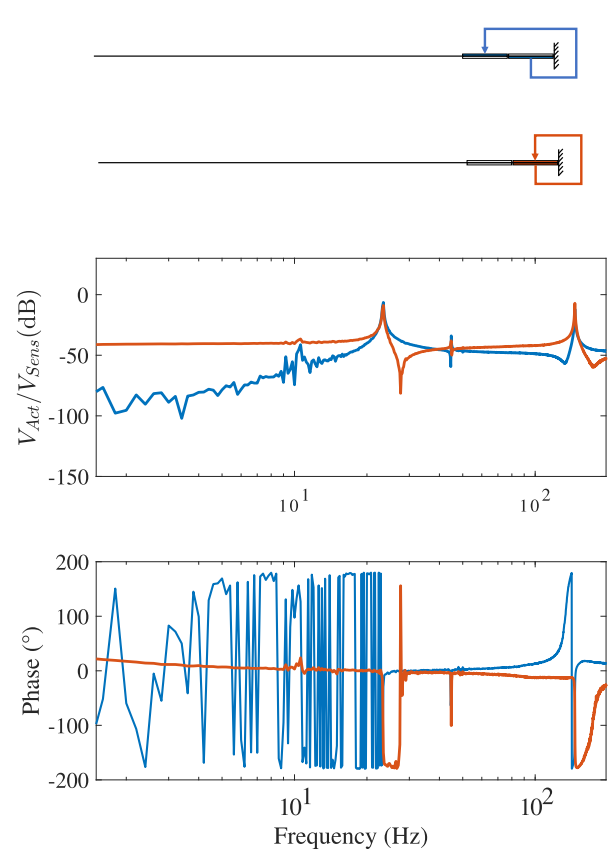

Figure 12. FRFs and phase evolutions between the voltage actuator and voltage sensor of the experimental cantilever beam in a collocated (━━) and a non-collocated (━━) setup.

Plant transfer functions

The system was excited from $1\,\mathrm{Hz}$ to $200\,\mathrm{Hz}$ via a multisine signal with a root-mean-square (rms) amplitude of $A = 0.5V$. The signal featured $N = 20000$ of samples per period, $P = 20$ periods and $R = 10$ realizations (Schoukens et al. 2016). The sampling rate was 4000 samples per second yielding in a frequency resolution of $0.2\,\mathrm{Hz}$. To build the FRF functions, the measurements were averaged over P and R. The measured plant transfer functions are displayed in Figure 12. The first resonance frequency at $23.2\,\mathrm{Hz}$ was targeted by the controller. The influence of the second and third mode at $44.8\,\mathrm{Hz}$ and $146\,\mathrm{Hz}$, respectively, was taken into account for the tuning. Based on the measured plant transfer functions, a state space model was built using the Matlab functions *tfest* and *tf2ss*. Figure 12 reveals that the FRF of the plant transfer function features small amplitudes before the first resonance in the non-collocated setup configuration, in line with the numerical simulations (cf. Figure 6). Both setups provide an alternating pole-zero pattern of the plant transfer functions. Comparing Figures 6 and 12, we note that there was a good agreement between the natural frequencies of the numerically-obtained and experimentally-identified open-loop plant transfer functions.

Damping performance

The PPF controller parameters were derived based on the identified state space model. The disturbance signal had an

rms amplitude of $A = 0.5V$ from $1\,\mathrm{Hz}$ to $200\,\mathrm{Hz}$ and the signal featured a 100000 samples per period, 20 periods and 10 realizations. The sampling rate was 10000 samples per second yielding a frequency resolution of $0.1\,\mathrm{Hz}$. Figure 13 presents the FRFs between the measured displacement and the disturbance voltage of the uncontrolled and controlled systems. The controller reduces the amplitude of the first resonance peak by $36\,\mathrm{dB}$ and $30\,\mathrm{dB}$ in the collocated and non-collocated cases, respectively. Due to the influence of the higher-order modes and possibly also of the static response, the expected two resonance peaks cannot clearly be seen in the FRF of the collocated setup. As already observed in the numerical simulations, the static response is strongly (not) amplified in the non-collocated (collocated) case. Overall, the performance of the PPF controller tuned with the H_∞ tuning rules can be regarded as highly satisfactory. Moreover, the controlled system exhibits phase margins of $-19.46°$ and $61.03°$ in the collocated and non-collocated cases, respectively (where a negative stability margin does not imply instability, as in Figure 4).
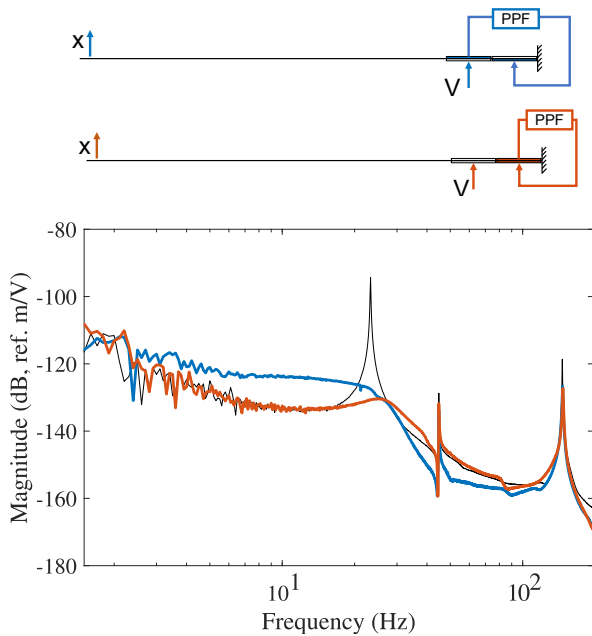

Figure 13. FRFs between the voltage actuator and voltage sensor of the experimental cantilever beam for the uncontrolled case (▬) and controlled by a PPF controller accounting for the influence of higher-order modes in a collocated (▬) and a non-collocated (▬) setup.

Comparison with the fixed-points method

Figure 14 evidences that both controllers lead to a satisfactory amplitude reduction, reducing the resonance amplitude by $36.5\,\mathrm{dB}$ (exact tuning rule) or $35.80\,\mathrm{dB}$ (fixed-points method). For the fixed-points method, two unbalanced resonance peaks appear around the resonance frequency. For the exact tuning rule, there is a single, more strongly-damped resonance peak.

Gain variations

Gain variations close to the value g_{opt} are presented in Figure 15(a). The close-up shows that the resonance
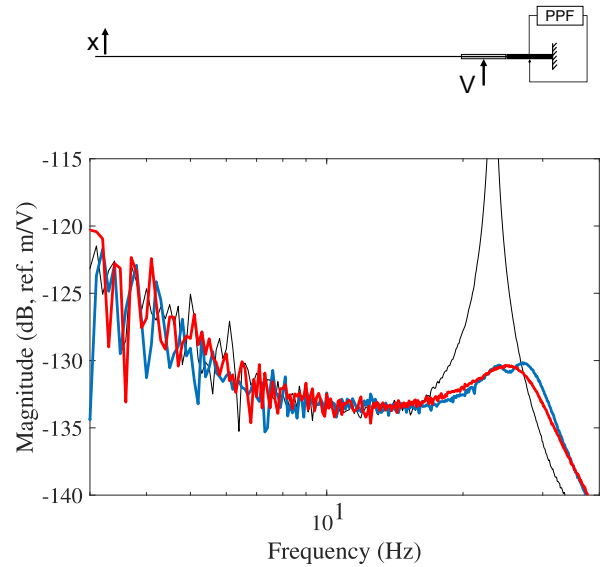

Figure 14. FRFs between the disturbance voltage and the tip displacement of the experimental cantilever beam for the uncontrolled case (▬) and controlled by a PPF controller tuned with exact H_∞ rules (▬) and with a fixed-points tuning (▬).

amplitude is more reduced using g_{max} instead of g_{opt}. Experimental uncertainties might explain this discrepancy with the theoretical developments, especially since g_{opt} and g_{max} are close to each other. Larger gain variations are shown in Figure 15(b). Damping performance is clearly the most effective close to g_{opt}. For gains significantly lower than this value, two resonance peaks are visible. This may be due to the fact that the resonance amplitude is greater than the static response.

As a final remark, we mention that taking the higher-order modes into account was not only essential for optimal damping but also to guarantee the controller's stability. When the controller was tuned without the the proposed correction procedure, the open-loop transfer function revealed that the controlled system would be unstable. Thus, the PPF controller could not have been implemented practically.

Conclusions and outlook

By exploiting the fact that the receptance functions of an RL shunt with an NC and a collocated PPF controller are equivalent, a new H_∞-based tuning rule was derived for a PPF controller. This strategy could yield a substantial reduction of the targeted resonance amplitude, sometimes at the cost of a growing static response. Thanks to the developed closed-form solution, this problem could be tackled and minimized. Our methodology was first demonstrated on an SDOF system, and its stability margins were analyzed by means of the open-loop transfer functions of the controlled systems. The optimal PPF controller exhibited sufficiently large stability margins, which makes it viable in practical applications.

Our developments also extend to the MDOF case thanks to a procedure that accounts for the influence of higher modes. It was shown that it is essential to include these
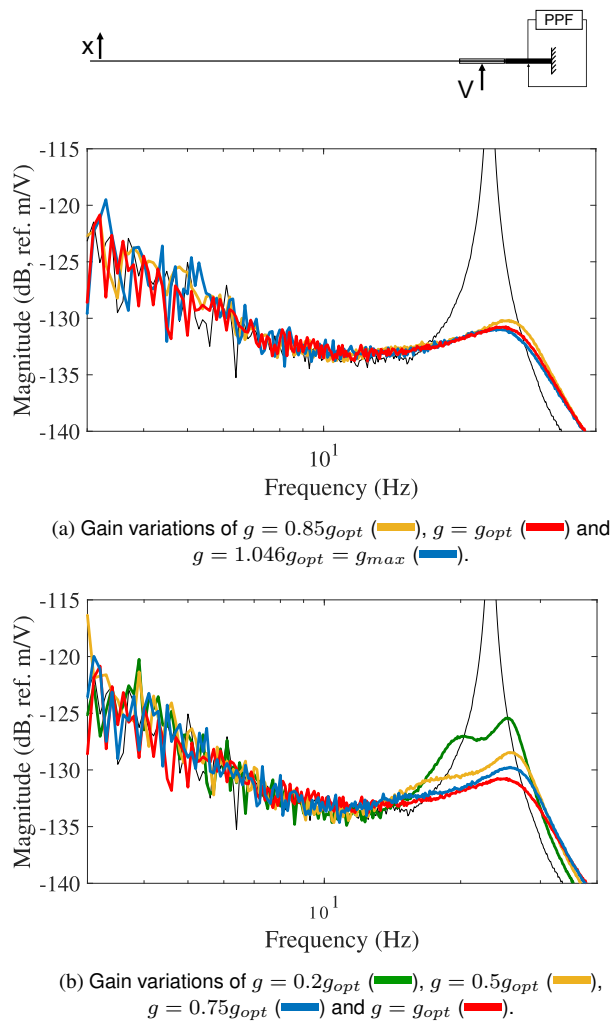
(a) Gain variations of $g = 0.85g_{opt}$ (▬), $g = g_{opt}$ (▬) and $g = 1.046g_{opt} = g_{max}$ (▬).

(b) Gain variations of $g = 0.2g_{opt}$ (▬), $g = 0.5g_{opt}$ (▬), $g = 0.75g_{opt}$ (▬) and $g = g_{opt}$ (▬).

Figure 15. FRFs between the structural response and the external disturbance voltage of the experimental cantilever beam controlled by a PPF controller with different gain settings in contrast to the uncontrolled response (▬).

modes for effective vibration mitigation. A numerical study on a cantilever beam using different actuator and sensor combinations was conducted, followed by an experimental verification. The outcome of these studies demonstrated the effectiveness of the controller with phase margins ensuring the stability of the controlled system.

The limitations of the approach were also discussed, especially in view of the equal-peak design in the controlled FRF. In the MDOF case, the controller performance varied with respect to the considered transfer function. Even if it might be possible to exactly enforce equal peaks in the receptance function, this is beyond the scope of this work. The presented approach provides rather a practical and easily applicable procedure to robustly design a PPF controller for an MDOF host structure.

This work establishes a basis for a new way of tuning a PPF controller for vibration control. Future works could include the consideration of lower modes when a higher mode is targeted or multiple modes are considered at the same time. In addition, the softening caused by the controller may decrease the frequency and amplify the amplitude of

modes with a lower frequency than the targeted one; this effect should be further investigated. Finally, the tuning rules could also be applied to real-life applications.

Declaration of competing interests

The authors declare no potential conflicts of interest with respect to the research, authorship, and/or publication of this article.

Funding

References

Agnes GS (1997) *Performance of Nonlinear Mechanical, Resonant-Shunted Piezoelectric, and Electronic Vibration Absorbers for Multi-Degree-of-Freedom Structures*. Doctoral Thesis, Virginia State University.

Amer YA, El-Sayed AT and Ahmed EE (2022) Vibration reduction of a non-linear ship model using positive position feedback controllers. *International Journal of Dynamics and Control* 10(2): 409–426. DOI:10.1007/s40435-021-00801-8. URL https://link.springer.com/10.1007/s40435-021-00801-8.

Balas MJ (1979) Direct Velocity Feedback Control of Large Space Structures. *Journal of Guidance and Control* 2(3): 252–253. DOI:10.2514/3.55869. URL https://arc.aiaa.org/doi/10.2514/3.55869.

Berardengo M, Thomas O, Giraud-Audine C and Manzoni S (2016) Improved resistive shunt by means of negative capacitance: new circuit, performances and multi-mode control. *Smart Materials and Structures* 25(7). DOI:10.1088/0964-1726/25/7/075033.

Clark RL (1997) Accounting for Out-of-Bandwidth Modes in the Assumed Modes Approach: Implications on Colocated Output Feedback Control. *Journal of Dynamic Systems, Measurement, and Control* 119(3): 390–395. DOI:10.1115/1.2801270.

de Marneffe B and Preumont A (2008) Vibration damping with negative capacitance shunts: theory and experiment. *Smart Materials and Structures* 17(3): 035015. DOI:10.1088/0964-1726/17/3/035015.

Dietrich J (2023) *Piezoelectric digital vibration absorbers for vibration mitigation of bladed structures*. Doctoral Thesis, University of Liège, Liège, Belgium. URL https://hdl.handle.net/2268/306077.

Dietrich J, Raze G, Collette C, Deraemaeker A and Kerschen G (2022) Resistive-inductive piezoelectric shunts with negative capacitances and positive position feedback - a comparative study. In: *Conference Proceedings of ISMA-USD2022*. Leuven, Belgium. URL https://hdl.handle.net/2268/294927.

Dosch J, Leo D and Inman D (1992a) Comparison of vibration control schemes for a smart antenna. In: *[1992] Proceedings*

of the 31st IEEE Conference on Decision and Control. Tucson, AZ, USA: IEEE. ISBN 978-0-7803-0872-5, pp. 1815–1820. DOI:10.1109/CDC.1992.371116. URL http://ieeexplore.ieee.org/document/371116/.

Dosch JJ, Inman DJ and Garcia E (1992b) A Self-Sensing Piezoelectric Actuator for Collocated Control. *Journal of Intelligent Material Systems and Structures* 3(1): 166–185. DOI:10.1177/1045389X9200300109. URL http://journals.sagepub.com/doi/10.1177/1045389X9200300109.

Fanson JL (1987) *An Experimental Investigation of Vibration Suppression in Large Space Structures Using Positive Position Feedback.* Doctoral Thesis, California Institute of Technology. DOI:10.7907/0SA8-HW86.

Fanson JL and Caughey TK (1990) Positive position feedback control for large space structures. *AIAA Journal* 28(4). DOI:10.2514/3.10451.

Fenik, S and Starek, L (2008) Optimal PPF controller for multimodal vibration mitigation. *Engineering MECHANICS* 15(3): p. 153–173.

Fleming A and Moheimani S (2005) Control orientated synthesis of high-performance piezoelectric shunt impedances for structural vibration control. *IEEE Transactions on Control Systems Technology* 13(1): 98–112. DOI:10.1109/TCST.2004.838547.

Franklin GF, Powell JD and Workman ML (1990) *Digital control of dynamic systems.* 2nd ed edition. Reading, Mass: Addison-Wesley. ISBN 978-0-201-11938-1.

Goh CJ and Caughey TK (1985) On the stability problem caused by finite actuator dynamics in the collocated control of large space structures. *International Journal of Control* 41(3): 787–802. DOI:10.1080/0020718508961163.

Gülbahçe E and Çelik M (2023) Frequency-Based Adaptive PPF Controller for Vibration Reduction of a Helicopter Shell Body. *Journal of Aerospace Engineering* 36(3): 1–9. DOI:10.1061/JAEEEZ.ASENG-4709. URL https://ascelibrary.org/doi/10.1061/JAEEEZ.ASENG-4709.

Hagood NW and von Flotow A (1991) Damping of structural vibrations with piezoelectric materials and passive electrical networks. *Journal of Sound and Vibration* 146(2). DOI:10.1016/0022-460X(91)90762-9.

Hamed Y, El Shehry A and Sayed M (2020) Nonlinear modified positive position feedback control of cantilever beam system carrying an intermediate lumped mass. *Alexandria Engineering Journal* 59(5): 3847–3862. DOI:10.1016/j.aej.2020.06.039. URL https://linkinghub.elsevier.com/retrieve/pii/S1110016820303094.

Hoffmeyer D and Høgsberg J (2020) Damping of coupled bending-torsion beam vibrations by spatially filtered warping position feedback. *Journal of Sound and Vibration* 477: 115323. DOI:10.1016/j.jsv.2020.115323.

Huertas VV and Rohaľ-Ilkiv B (2012) Vibration Suppression of a Flexible Structure. *Procedia Engineering* 48: 233–241. DOI:10.1016/j.proeng.2012.09.509.

Høgsberg J and Krenk S (2017) Calibration of piezoelectric RL shunts with explicit residual mode correction. *Journal of Sound and Vibration* 386: 65–81. DOI:10.1016/j.jsv.2016.08.028.

Ikegame T, Takagi K and Inoue T (2019) Exact Solutions to H_∞ and H_2 Optimizations of Passive Resonant Shunt Circuit for Electromagnetic or Piezoelectric Shunt Damper. *Journal of Vibration and Acoustics* 141. DOI:10.1115/1.4042819.

Inman DJ (2006) *Vibration with control.* Hoboken, NJ: Wiley. ISBN 978-0-470-01051-8.

Krenk S and Høgsberg J (2013) Equal modal damping design for a family of resonant vibration control formats. *Journal of Vibration and Control* 19(9): 1294–1315. DOI:10.1177/1077546312446796. URL http://journals.sagepub.com/doi/10.1177/1077546312446796.

Kwak MK and Han SB (1998) Application of genetic algorithms to the determination of multiple positive-position feedback controller gains for smart structures. San Diego, CA, pp. 637–648. DOI:10.1117/12.316341.

MacLean J, Aleyaasin M and Aphale SS (2022) How Far Should Poles Be Placed? Selecting Positive Feedback Controllers for Damping and Tracking Applications: A Complete Characterisation. *Vibration* 5(4): 641–658. DOI:10.3390/vibration5040038. URL https://www.mdpi.com/2571-631X/5/4/38.

Marinangeli L, Alijani F and HosseinNia SH (2018) Fractional-order positive position feedback compensator for active vibration control of a smart composite plate. *Journal of Sound and Vibration* 412: 1–16. DOI:10.1016/j.jsv.2017.09.009.

Mokrani B (2022) Active vibration isolation with positive position feedback, Oral presentation at ISMA-USD2022.

Niu W, Li B, Xin T and Wang W (2018) Vibration active control of structure with parameter perturbation using fractional order positive position feedback controller. *Journal of Sound and Vibration* 430: 101–114. DOI:10.1016/j.jsv.2018.05.038.

Paknejad A, Zhao G, Osée M, Deraemaeker A, Robert F and Collette C (2020) A novel design of positive position feedback controller based on maximum damping and H_2 optimization. *Journal of Vibration and Control* 26(15-16). DOI:10.1177/1077546319892755.

Preumont A (2011) *Vibration Control of Active Structures*, *Solid Mechanics and Its Applications*, volume 179. 3 edition. Dordrecht: Springer Netherlands. ISBN 978-94-007-2032-9. DOI:10.1007/978-94-007-2033-6.

Preumont A, Dufour JP and Malekian C (1992) Active damping by a local force feedback with piezoelectric actuators. *Journal of Guidance, Control, and Dynamics* 15(2): 390–395. DOI:10.2514/3.20848.

Raze G, Dietrich J and Kerschen G (2021) Passive control of multiple structural resonances with piezoelectric vibration absorbers. *Journal of Sound and Vibration* 515: 116490. DOI:10.1016/j.jsv.2021.116490.

Raze G, Dietrich J and Kerschen G (2022) Tuning and performance comparison of multiresonant piezoelectric shunts. *Journal of Intelligent Material Systems and Structures* : 1045389X2210880DOI:10.1177/1045389X221088031.

Raze G, Jadoul A, Guichaux S, Broun V and Kerschen G (2020) A digital nonlinear piezoelectric tuned vibration absorber. *Smart Materials and Structures* 29(1). DOI:10.1088/1361-665X/ab5176.

Russell D, San-Millan A, Feliu V and Aphale SS (2016) Butterworth Pattern-based Simultaneous Damping and Tracking Controller Designs for Nanopositioning Systems. *Frontiers in Mechanical Engineering* 2. DOI:10.3389/fmech.2016.00002. URL http://journal.frontiersin.org/article/10.3389/fmech.2016.00002.

Saeed NA, Awwad EM, Abdelhamid T, El-Meligy MA and Sharaf M (2021) Adaptive versus Conventional Positive

Position Feedback Controller to Suppress a Nonlinear System Vibrations. *Symmetry* 13(2): 255. DOI:10. 3390/sym13020255. URL https://www.mdpi.com/2073-8994/13/2/255.

Schoukens J, Vaes M and Pintelon R (2016) Linear System Identification in a Nonlinear Setting: Nonparametric Analysis of the Nonlinear Distortions and Their Impact on the Best Linear Approximation. *IEEE Control Systems* 36(3): 38–69. DOI:10.1109/MCS.2016.2535918.

Silva TM, Hameury C, Ferrari G, Balasubramanian P, Franchini G and Amabili M (2023) Particle swarm optimization of a non-collocated MIMO PPF active vibration control of a composite sandwich plate. *Journal of Sound and Vibration* 555(March): 117723. DOI:10.1016/j.jsv.2023. 117723. URL https://linkinghub.elsevier.com/retrieve/pii/S0022460X23001724.

Soltani P, Kerschen G, Tondreau G and Deraemaeker A (2014) Piezoelectric vibration damping using resonant shunt circuits: an exact solution. *Smart Materials and Structures* 23(12). DOI: 10.1088/0964-1726/23/12/125014.

Thomas O, Deü JF and Ducarne J (2009) Vibrations of an elastic structure with shunted piezoelectric patches: efficient finite element formulation and electromechanical coupling coefficients. *International Journal for Numerical Methods in Engineering* 80(2): 235–268. DOI:10.1002/nme.2632.

Toftekær JF, Benjeddou A and Høgsberg J (2020) General numerical implementation of a new piezoelectric shunt tuning method based on the effective electromechanical coupling coefficient. *Mechanics of Advanced Materials and Structures* 27(22): 1908–1922. DOI:10.1080/15376494.2018.1549297.

Visalakshi V, Khare S, Moheimani SOR and Bhikkaji B (2021) Design of Positive Position Feedback Controllers for Collocated Systems. In: *2021 American Control Conference (ACC)*, volume 2021-May. IEEE. ISBN 978-1-6654-4197-1, pp. 4791–4796. DOI:10.23919/ACC50511.2021. 9482878. URL https://ieeexplore.ieee.org/document/9482878/.

Wolfram Research Inc (2022) Mathematica, Version 12.2. URL https://www.wolfram.com/wolfram-alpha-notebook-edition. Champaign, IL.

Yuan B, Meng Z and Dong RQ (2024) Design of anti-unwinding attitude coupling controller for flexible spacecraft using positive position feedback control. *Acta Astronautica* 218(February): 163–176. DOI:10.1016/j.actaastro.2024.02. 018. URL https://linkinghub.elsevier.com/retrieve/pii/S0094576524000821.

Zhao G, Paknejad A, Raze G, Deraemaeker A, Kerschen G and Collette C (2019) Nonlinear positive position feedback control for mitigation of nonlinear vibrations. *Mechanical Systems and Signal Processing* 132: 457–470. DOI:10.1016/j.ymssp.2019. 07.005.

Zhao G, Paknejad A, Raze G, Kerschen G and Collette C (2018) H_∞ optimization of positive position feedback control for mitigation of nonlinear vibrations. In: *Conference Proceedings of ISMA2018 - USD2018*. Leuven.